

Effective Field Neural Network

Xi Liu,¹ Yujun Zhao,¹ Chun Yu Wan,¹ Yang Zhang,^{2,3} and Junwei Liu^{1,*}

¹*Department of Physics, Hong Kong University of Science and Technology, Clear Water Bay, Hong Kong SAR, China*

²*Department of Physics and Astronomy, University of Tennessee, Knoxville, TN 37996, USA*

³*Min H. Kao Department of Electrical Engineering and Computer Science,*

University of Tennessee, Knoxville, Tennessee 37996, USA

(Dated: February 26, 2025)

In recent years, with the rapid development of machine learning, physicists have been exploring its new applications in solving or alleviating the curse of dimensionality in many-body problems. In order to accurately reflect the underlying physics of the problem, domain knowledge must be encoded into the machine learning algorithms. In this work, inspired by field theory, we propose a new set of machine learning models called effective field neural networks (EFNNs) that can automatically and efficiently capture important many-body interactions through multiple self-refining processes. Taking the classical 3-spin infinite-range model and the quantum double exchange model as case studies, we explicitly demonstrate that EFNNs significantly outperform fully-connected deep neural networks (DNNs) and the effective model. Furthermore, with the help of convolution operations, the EFNNs learned in a small system can be seamlessly used in a larger system without additional training and the relative errors even decrease, which further demonstrates the efficacy of EFNNs in representing core physical behaviors.

The collective behaviors of many interacting particles—such as spins, molecules, and atoms—give rise to some of the most intriguing phenomena in condensed matter physics. However, theoretical and computational studies of many-body problems often confront the curse of dimensionality and one must devise strategies to circumvent it. Machine learning has emerged as a powerful tool for extracting effective features from high-dimensional datasets, garnering significant attention for its ability to tackle long-standing problems in condensed matter physics. Numerous machine learning techniques have been applied to a wide range of classical and quantum many-body systems, including classifying phases of matter with supervised [1–3] and unsupervised machine learning [4–8], representing many-body quantum states [9–13], accelerating Monte-Carlo simulations [14–17], fitting high-dimensional potential energy surfaces [18–22] and searching for spin glass ground states [23].

Standard deep neural networks (DNNs) have been shown to be ineffective in solving many-body problems unless augmented with physical knowledge. For example, mapping the spin configuration to energy in an 8×8 classical two-dimensional Ising model requires highly complex DNN structures [24]. Consequently, extensive research has focused on encoding physics into neural network architectures to enhance their effectiveness in physical applications, such as incorporating physical laws [25–28] and physical constraints [29, 30], mimicking physical processes [31], accounting for symmetry [32] and integrating graph structure in atomic bonding [33–39], employing renormalization group procedures [40]. These physics-encoded neural networks have found applications in computing effective Hamiltonians [41–43], property predic-

tion [36, 39, 41, 43–49], structure search [37, 38], etc. These methods, although often outperforming standard DNNs, tend to rely on intuitive and simplified imitations of physical principles, and still remain elusive in revealing the underlying the many-body interactions.

In this work, inspired by field theory, we propose a new class of machine learning models, called effective field neural networks (EFNNs). The core motivation is to decompose many-body interactions into single quasi-particle representations governed by an emergent effective field. Different from standard DNNs, where an adjacent layer relies only on the previous layer, EFNNs incorporate the initial feature values at every layer to form the self-similarity structure with parameters trains via a recursive self-refining process, in the spirit of renormalization group theory, and hence can effectively capture the underlying physics of many-body interactions. Unlike approaches such as FermiNet [50], which directly parameterizes high-dimensional wave-functions without explicit separation of quasi-particles and fields, our method does not presuppose a fixed ansatz for the wavefunction. Instead, the quasi-particle and effective field representations are learned through an recursive self-refining process, mirroring the renormalization group (RG) framework in field theory, while leveraging the expressive power of deep neural networks. This recursive approach progressively refines the accuracy of both the quasi-particle and effective field descriptions.

We first illustrate the EFNN architecture by reformulating the classical 2D Ising model within the EFNN framework. The Hamiltonian of a classical 2D Ising model is defined as $H(S) = -J \sum_{\langle ij \rangle} s_i s_j$, where $\langle ij \rangle$ denotes a summation over pairs of nearest-neighbor sites, $s_i = \pm 1$ represents the spin at site i , J is the interaction strength between two spins, and S is the collection of all spins. First, we define the effective field on spin s_i as $\phi_i(S)$, which is equal to the sum of the nearest neigh-

* liuj@ust.hk

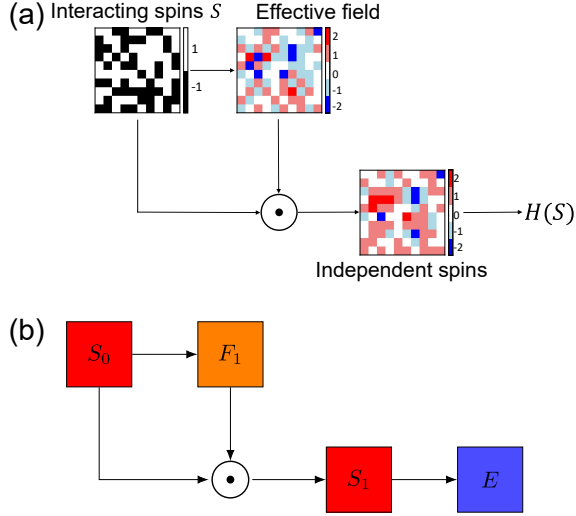


FIG. 1. Energy evaluation of a 2D Ising model reformulated as a neural network. (a) Calculation of the effective field by summing the interacting spins. Each interacting spin is multiplied by its corresponding effective field to obtain independent spin values, and the total energy is determined by summing up these independent spins. (b) Neural network representation of the energy evaluation process. \odot represents the element-wise multiplication.

bor spins of s_i multiplied by $-\frac{J}{2}$. Then, we define the independent spin (quasi-particle) as $s_i\phi_i(S)$, hence the total energy reads $H(S) = \sum_i s_i\phi_i(S)$. As illustrated schematically in Fig. 1(a), the interacting spins are first mapped to an effective field, then the effective field combining with the interacting spins is mapped to independent spins. Finally, a summation is performed over the independent spins, and the total energy is obtained. We reformulate the computational procedure within a DNN-like structure, depicted in Fig. 1(b). Here, $S_0 = S$ is the input layer, representing the interacting spins. The effective field layer F_1 and the quasi-particle layer S_1 constitute a single field-particle (FP) layer. The evaluation of S_1 relies on both the effective layer F_1 and the interacting spin layer S_0 , therefore a connection is required from S_0 to S_1 , as well as from F_1 to S_1 , distinguishing this architecture from a standard DNN. Finally, a summation is performed over S_1 to obtain the energy E .

In the classical 2D Ising model, both the effective field and quasi-particles can be exactly calculated, which, however, becomes infeasible for more complex many-body interactions. Following the spirit of renormalization from field theory, we can recursively refine the evaluations of the effective field and the quasi-particles. As shown in Fig. 2(a), we can extend the FP layer number in Fig. 1(b) to obtain the deep effective field neural networks. The evaluation procedure is detailed as

$$F_i = f_{i-1}(S_{i-1}), S_i = g_i(S_0) \odot F_i, E = q(S_n),$$

where the function f_{i-1} maps the previous quasi-particle layer S_{i-1} (for $i \geq 2$) or the initial layer S_0 (for $i = 1$)

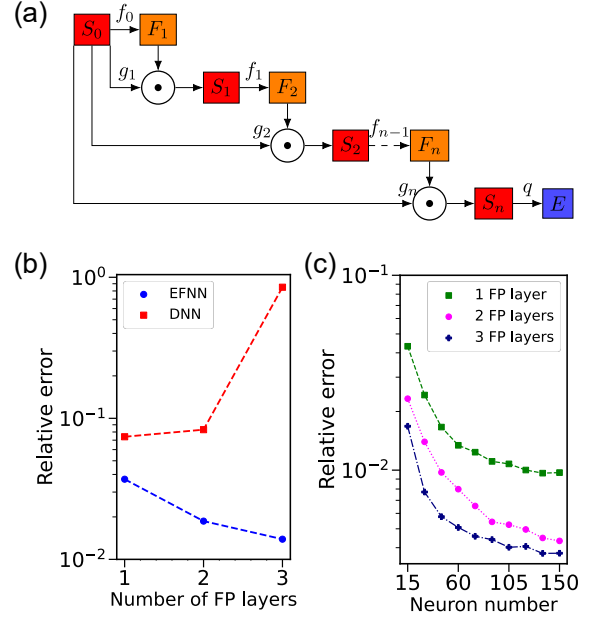


FIG. 2. Performance of EFNNs on a classical 3-spin infinite range model. (a) Architecture of the EFNN. (b) Performance of EFNNs and DNNs on the test set. (c) Performance of EFNNs as the neuron number increases.

to the effective field layer F_i . The input layer S_0 is first processed by g_i , then multiplied in elements by F_i to produce the quasi-particle layer S_i . Each FP layer consists of F_i and S_i . The final quasi-particle layer S_n generates the output energy E through the function q , which sums all elements of the last layer. Typically, f_i and g_j are nonlinear to enhance expressiveness, though linear functions may suffice for simpler models like the classical 2D Ising model with nearest-neighbor interactions.

We present two case studies to demonstrate the capability of EFNNs to capture many-body interactions. The first case study focuses on the classical 3-spin infinite range model in 1D, with Hamiltonian:

$$H(S) = - \sum_{i < j < k} J_{ijk} s_i s_j s_k, \quad (1)$$

where the spins take binary values 0, 1, J_{ijk} are constants, and the system comprises 15 lattice sites. We train EFNNs to evaluate $H(S)$ in Eq. (1), and compare its performance with that of DNNs.

We generate 16000 training and 4000 test samples using Eq. (1). Utilizing the EFNN architecture in Fig. 2(a), the nonlinear mappings f_i and g_j are constructed by sequential linear layers with tanh activations. The network is trained with the Adam optimizer and a decaying learning rate. Performance is evaluated by the relative error, defined as the square root of the MSE on the test set divided by the absolute mean of $H(S)$. We compare EFNNs to standard DNNs, using 18 neurons per layer and varying the number of FP layers ($n = 1, 2, 3$). With one FP layer, the DNN achieves approximately a 7×10^{-2}

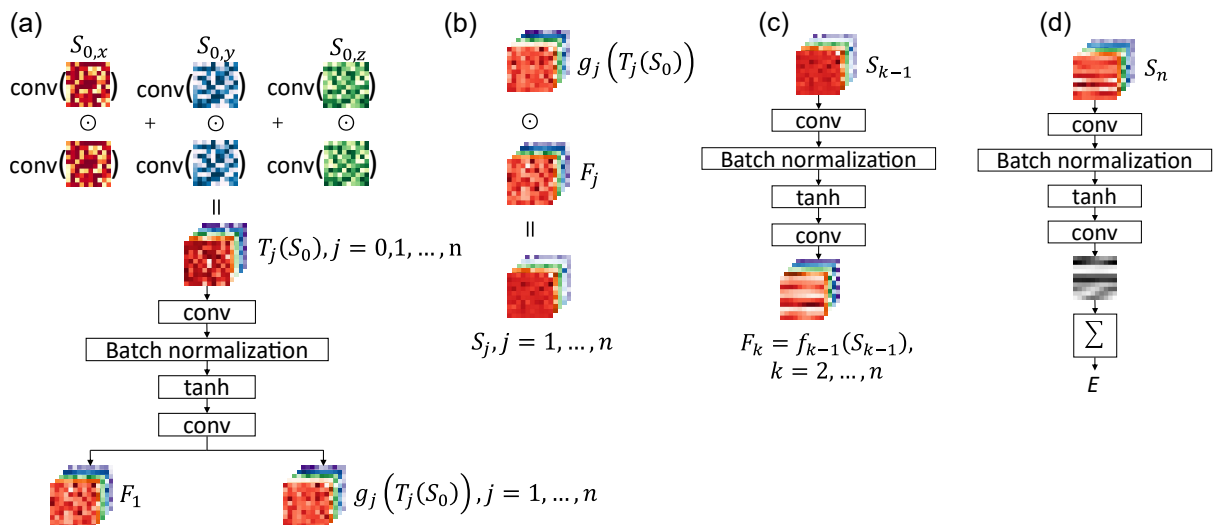


FIG. 3. Computational workflow of EFNNs with symmetrization. (a) Symmetrization: Each of the three channels of S_0 ($S_{0,x}$, $S_{0,y}$, $S_{0,z}$) undergoes convolution and element-wise multiplication within the same channel. The resulting products are summed to form the symmetrization layer $T_j(S_0)$. Subsequently, $T_j(S_0)$ is passed through a sequence of layers—convolution, batch normalization, tanh activation, and another convolution—to produce F_1 for $j = 0$ or $g_j(T_j(S_0))$ for $j = 1, \dots, n$. (b) Generation of quasi-particle layers: The transformed symmetrization layer $g_j(T_j(S_0))$ is element-wise multiplied with the effective field layer F_j , resulting in the quasi-particle layer S_j , $j = 1, \dots, n$. (c) Transformation to effective field layers: Each quasi-particle layer S_{k-1} is processed through convolution, batch normalization, tanh activation, and another convolution to generate the effective field layer F_k , for $k = 2, \dots, n$. (d) Energy evaluation: The final quasi-particle layer S_n is transformed into a single-channel matrix. An element-wise summation of this matrix yields the scalar energy prediction E . These images are generated after training the model with $C = 10$ channels and $n = 2$ layers. Only the first five channels are displayed for clarity, using the 576th sample from the test set as input S_0 .

relative error, while the EFNN attains around 4×10^{-2} . As the number of FP layers increases, the DNN's error rapidly worsens, whereas the EFNN's error decreases to about 1×10^{-2} with three FP layers (Fig. 2(b)). Additionally, Fig. 2(c) shows that increasing the number of neurons in the EFNN from 15 to 150 leads to an algebraic decrease in relative error, reaching a minimum around 150 neurons for all tested FP layers, and optimal performance is achieved with three FP layers. These results demonstrate that EFNNs effectively capture many-body interactions through multiple feed-forward paths, improving accuracy as layers and neurons increase. In contrast, DNNs lose their ability to fit the energy accurately with additional layers. Both the number of FP layers and the internal neuron count are crucial for the EFNNs' high performance.

We proceed to our second, more challenging case study: evaluating the Monte-Carlo energy of the quantum double exchange model [51–53] at finite temperature. The Hamiltonian on an $N \times N$ lattice reads

$$H(S) = -t \sum_{\langle i,j \rangle, \alpha} \left(\hat{c}_{i\alpha}^\dagger \hat{c}_{j\alpha} + \text{h.c.} \right) - \frac{J}{2} \sum_{i, \alpha, \beta} \vec{s}_i \cdot \hat{c}_{i\alpha}^\dagger \vec{\sigma}_{\alpha\beta} \hat{c}_{i\beta}, \quad (2)$$

where $\langle ij \rangle$ denotes nearest neighbors, $\hat{c}_{i\alpha}$ is the fermion annihilation operator with spin α at site i , $\vec{\sigma}$ are the Pauli matrices, and $\vec{s}_i \in \mathbb{S}^2$ is a 3D classical unit vector

representing the local spin at site i , the classical spin interacts with the fermions through an on-site coupling, and S is the collection of all classical spins \vec{s}_i . We set $N = 10$, $J = 16t$, $\mu = -8.3t$, $T = 0.1t$, $t = 1$.

At finite temperature T , the Monte-Carlo energy is defined as $E_{\text{MC}}(S) = -T \sum_n \log(1 + e^{-\frac{1}{T} E_n(S)})$, where $\{E_n(S)\}$ are the eigen-energies of $H(S)$ in Eq. (2) for a given spin configuration S . This quantity proves to be useful in Monte-Carlo simulations of the double exchange model, as it can replace exact diagonalization in Determinant Quantum Monte Carlo (DQMC) computations [54]. Diagonalizing a $2N^2 \times 2N^2$ Hermitian matrix for Eq. (2) has a computational complexity of $O(N^6)$ for each spin update. Both effective models and neural networks can significantly reduce this complexity. We compare the performance of an effective model incorporating 4-body RKKY-type interactions [55–57] with that of EFNNs adopting symmetrization. The effective model is expressed as

$$E_{\text{eff}}(S) \sim J_0 + \sum_{ij} g_{ij} \vec{s}_i \cdot \vec{s}_j + \sum_{ijkl} g_{ijkl} (\vec{s}_i \cdot \vec{s}_j) (\vec{s}_k \cdot \vec{s}_l). \quad (3)$$

Here, the dot products include all pairs of spins on the lattice, including self-interactions. Clearly, the number of parameters factorially increases with N and the effective model cannot be solved exactly for a large N . To simplify,

we divide the 10×10 lattice into four 5×5 tiles, restricting two- and four-body interactions within each tile.

The spin interactions in Eq. (3) are exclusively expressed as dot products to satisfy the $O(3)$ symmetry of Eq. (2). Inspired by this symmetry, we incorporate symmetrization layers into the EFNN architecture, depicted in Fig. 3(a). The symmetrization is achieved by summing dot products of each channel of S_0 after convolution:

$$T_j(S_0) = \sum_{k=x,y,z} \text{conv}(S_{0,k}) \odot \text{conv}(S_{0,k}), \quad j = 0, 1, \dots, n.$$

Here, each $S_{0,k} \in \mathbb{R}^{N \times N}$ is convolved into $\mathbb{R}^{C \times N \times N}$. Supplementary Material [58] details the convolution process and proves that T_j remains invariant under $O(3)$ transformations. As shown in Fig. 4(a), in the first FP layer, F_1 and S_1 are initialized as

$$F_1 = f_0(T_0(S_0)), \quad S_1 = g_1(T_1(S_0)) \odot F_1.$$

For subsequent layers $j = 2, \dots, n$, the effective field and quasi-particle layers are

$$F_j = f_{j-1}(S_{j-1}), \quad S_j = g_j(T_j(S_0)) \odot F_j.$$

The mappings f_j and g_k consist of a convolutional layer, batch normalization, a tanh activation, and another convolutional layer. Fig. 3 illustrates the computational workflow: (a) symmetrization, (b) generation of quasi-particle layers, (c) transformation to effective field layers for subsequent FP layers, and (d) evaluation of energy. For the energy function q , after passing through the aforementioned layers, an extra summation layer generates a scalar value as the predicted energy. Specifically, the final quasi-particle layer S_n is transformed into a single-channel matrix, and an element-wise summation is performed to produce the scalar energy prediction E , as shown in Fig. 3(d). The layer dimensions are as follows: input layer $S_0 \in \mathbb{R}^{3 \times N \times N}$, intermediate layers $F_j, S_j \in \mathbb{R}^{C \times N \times N}$, for $j = 1, \dots, n$, and output $E = q(S_n) \in \mathbb{R}$.

We generate a total of 2×10^6 data points and split them into 80% for training and 20% for testing. These data are obtained by exact diagonalization of the Hamiltonian in Eq. (2). For the effective model in Eq. (3), we perform a linear regression to obtain the coefficients. The EFNNs with symmetrization are trained using networks with $C = 10, 15, 20, 25$ channels and $n = 1, 2, 3$ FP layers. As shown in Fig. 4(b), the effective model achieves a relative error of approximately 2×10^{-2} . In contrast, the EFNNs with symmetrization consistently reduce the relative error below 3×10^{-3} as C increases from 10 to 25, for $n = 1, 2, 3$. Notably, the EFNNs outperform the effective model by a factor of six while utilizing significantly fewer parameters, underscoring their capability to capture high-order interactions in quantum many-body systems. Their parameter count scales as $O(nC^2)$, resulting in 26250, 49560, and 72870 parameters for $n = 1, 2, 3$ at $C = 10$. In stark contrast, the perturbative expansion in

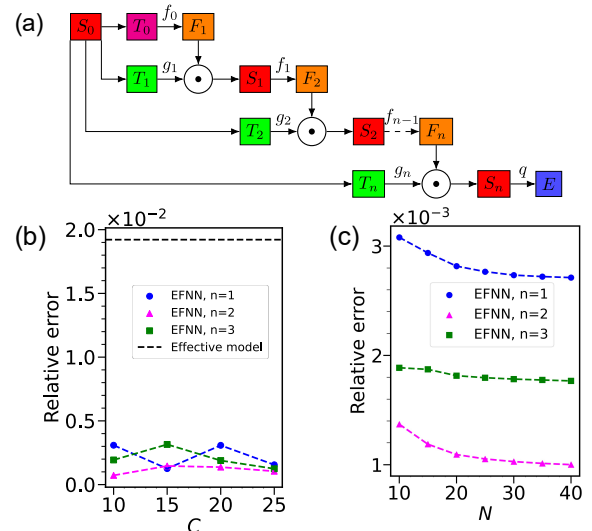


FIG. 4. Relative error of EFNNs. (a) Architecture of EFNN incorporating symmetrization layers T_j , $j = 0, 1, \dots, n$. (b) Comparison of EFNNs' and the effective model's performance on a test set with lattice size $N = 10$, for channel numbers $C = 10, 15, 20, 25$. (c) Performance of the EFNN model, trained on a 10×10 lattice with $C = 20$ channels, when applied to larger lattice systems.

Eq. (3) scales factorially as $O\left(\frac{1}{\frac{1}{2}k} \left(\frac{1}{2}N^4 + \frac{1}{2}N^2 + \frac{1}{2}k - 1\right)\right)$, with k denoting the interaction order—a scaling that can lead to divergence at higher orders. The full effective model in Eq. (3) contains 12758826 parameters, which reduces to 213201 when interactions are restricted within each tile. Furthermore, EFNNs effectively select the most significant interactions automatically, an essential aspect of renormalization. By renormalizing the interactions and prioritizing key terms, EFNNs avoid both divergence and explosive growth in the number of parameters.

We further assess the extrapolation performance of EFNNs with symmetrization with the model trained on a 10×10 lattice and tested on systems of $N = 15, 20, 25, 30, 35$, and 40. Using the relative error of energy as the performance metric, Fig. 4(c) illustrates that for $N = 10$, all EFNNs accurately predict the energy, consistent with Fig. 4(b). As the lattice size increases, the relative error slightly decreases for all FP layers with $n = 1, 2, 3$. This occurs because the absolute error increases only marginally with N , while the absolute value of the average energy grows significantly, thereby reducing the relative error. Moreover, EFNNs with $n = 2$ and $n = 3$ FP layers outperform those with a single FP layer, demonstrating enhanced renormalization capability with additional layers. Notably, even for larger systems, all models maintain relative errors below 3×10^{-3} , with the $n = 2$ configuration achieving a minimum relative error of 1×10^{-3} . These results underscore the EFNN's efficacy: the convolution operations with padding under boundary condition PBC effectively capture interactions

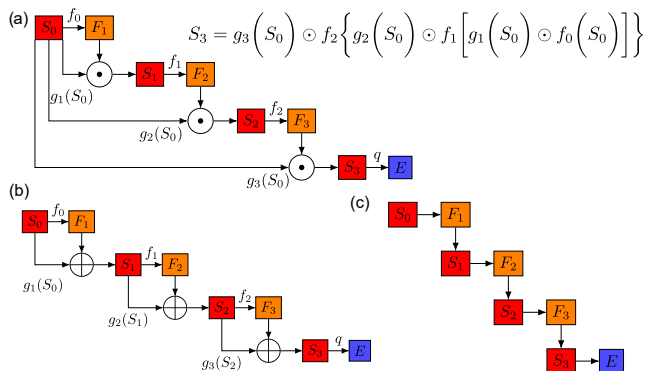


FIG. 5. Continued function representation of an EFNN with 3 FP layers. (a) In an EFNN, the initial layer S_0 is recursively integrated into every quasi-particle layer. After a mapping, S_0 is multiplied with subsequent layers, forming a continued function representation (see right-hand side equation). (b) A typical architecture of ResNet, only one skip connection starts from S_0 and summation is used, which limits its renormalization capability. (c) Removing the S_0 connections transforms an EFNN into a standard DNN, where S_0 only appears at the beginning of the iterations, resulting in significantly diminished expressive power.

between localized and neighboring spins, and the renormalization through multiple FP layers ensures robust energy predictions across varying lattice sizes.

We give some discussions and conclude this paper. In both case studies, we have demonstrated that increasing the number of layers and neurons (or channels in convolutional layers) enhances the neural network’s accuracy, aligning with well-established findings in fields like computer vision. EFNN’s self-similar structure mirrors the renormalization process—a non-perturbative method for evaluating complicated functions, such as the Yang-Mills β function [59] or Becke’s correction to the LDA functional in DFT [60]. This approximation framework stems from Padé approximants [61] using rational functions, which can also be expressed as continued fractions—an important and specific example of continued functions [62], known for superior convergence with much fewer parameters [63–66]. Actually, EFNNs possess exactly the structure of continued functions, as shown in Fig. 5(a). In an EFNN, the initial feature layer S_0 connects recursively to every quasi-particle layer via mappings g_j ; each nonlinear mapping f_{j-1} is multiplied with $g_j(S_0)$. In addition, EFNNs employ the tanh activa-

tion function within their renormalization-like structure, making them compatible with standard deep learning frameworks and enabling training via stochastic gradient descent with back-propagation. This contrasts with Padé approximants, which typically use the inverse function and hence usually determine parameters through perturbative series matching due to potential singularity in the gradient descent. As shown in Fig. 5(b), ResNets [67–70] adopt a similar but fundamentally different skip-like connections from EFNNs. In a ResNet, S_0 is skip-connected to later layers only once, with later skip connections starting in the middle, and its summation-based aggregation fails to meet the continued function formulation—resulting in suboptimal performance to characterize the many-body interactions. Standard DNNs (Fig. 5(c)) lack skip connections entirely, and S_0 only appears in the beginning of iterations, resulting in a very limited expressive capability. Moreover, by partitioning intermediate layers into effective field and quasi-particle layers, EFNNs provide a clear physical interpretation: quasi-particles emerge from the dot product of interacting particles (via a mapping) and effective fields, which is absent in ResNets and standard DNNs.

In conclusion, inspired by field theory, we have proposed a novel deep neural network architecture called EFNN, which effectively captures high-order interactions in both classical and quantum models. EFNN’s high accuracy and efficiency arise from the recursive refinement of effective fields and the construction of quasi-particles that encapsulate complex many-body effects. As discussed earlier, the connections from the true particle layer S_0 to the quasi-particle layers (or the preceding symmetrization layers) establish a structure of continued functions, and have renormalization power analogous to Padé approximants. Once the effective fields and quasi-particles are properly renormalized, the trained model can accurately predict the energy for a system with complicated many-body interactions. Furthermore, EFNNs maintain high accuracy even when applied to significantly larger systems. In future work, we aim to integrate Padé approximation and continued function theories more rigorously into the EFNN framework and derive error estimates for the neural network’s predictions.

Acknowledgments—This work is supported by the Hong Kong Research Grants Council (16306220) and National Key R&D Program of China (2021YFA1401500). Y.Z. is supported by the Max Planck Partner lab on quantum materials from Max Planck Institute Chemical Physics of Solids.

[1] J. Carrasquilla and R. G. Melko, Machine learning phases of matter, *Nature Physics* **13**, 431 (2017).
 [2] K. Ch’ng, J. Carrasquilla, R. G. Melko, and E. Khatami, Machine Learning Phases of Strongly Correlated Fermions, *Phys. Rev. X* **7**, 031038 (2017).
 [3] I. A. Iakovlev, O. M. Sotnikov, and V. V. Mazurenko,

Supervised learning approach for recognizing magnetic skyrmion phases, *Phys. Rev. B* **98**, 174411 (2018).
 [4] L. Wang, Discovering phase transitions with unsupervised learning, *Phys. Rev. B* **94**, 195105 (2016).
 [5] E. P. L. van Nieuwenburg, Y.-H. Liu, and S. D. Huber, Learning phase transitions by confusion, *Nature Physics*

- 13**, 435 (2017).
- [6] K. Ch'ng, N. Vazquez, and E. Khatami, Unsupervised machine learning account of magnetic transitions in the Hubbard model, *Phys. Rev. E* **97**, 013306 (2018).
- [7] J. F. Rodriguez-Nieva and M. S. Scheurer, Identifying topological order through unsupervised machine learning, *Nature Physics* **15**, 790 (2019).
- [8] J. Arnold, F. Schäfer, M. Žonda, and A. U. J. Lode, Interpretable and unsupervised phase classification, *Phys. Rev. Res.* **3**, 033052 (2021).
- [9] G. Carleo and M. Troyer, Solving the quantum many-body problem with artificial neural networks, *Science* **355**, 602 (2017).
- [10] Y. Nomura, A. S. Darmawan, Y. Yamaji, and M. Imada, Restricted Boltzmann machine learning for solving strongly correlated quantum systems, *Phys. Rev. B* **96**, 205152 (2017).
- [11] K. Choo, G. Carleo, N. Regnault, and T. Neupert, Symmetries and Many-Body Excitations with Neural-Network Quantum States, *Phys. Rev. Lett.* **121**, 167204 (2018).
- [12] N. Yoshioka and R. Hamazaki, Constructing neural stationary states for open quantum many-body systems, *Phys. Rev. B* **99**, 214306 (2019).
- [13] J. Carrasquilla, G. Torlai, R. G. Melko, and L. Aolita, Reconstructing quantum states with generative models, *Nature Machine Intelligence* **1**, 155 (2019).
- [14] J. Liu, Y. Qi, Z. Y. Meng, and L. Fu, Self-learning Monte Carlo method, *Phys. Rev. B* **95**, 041101 (2017).
- [15] J. Liu, H. Shen, Y. Qi, Z. Y. Meng, and L. Fu, Self-learning Monte Carlo method and cumulative update in fermion systems, *Phys. Rev. B* **95**, 241104 (2017).
- [16] L. Huang and L. Wang, Accelerated Monte Carlo simulations with restricted Boltzmann machines, *Phys. Rev. B* **95**, 035105 (2017).
- [17] G. Kanwar, M. S. Albergo, D. Boyda, K. Cranmer, D. C. Hackett, S. Racanière, D. J. Rezende, and P. E. Shanahan, Equivariant Flow-Based Sampling for Lattice Gauge Theory, *Phys. Rev. Lett.* **125**, 121601 (2020).
- [18] J. Behler and M. Parrinello, Generalized Neural-Network Representation of High-Dimensional Potential-Energy Surfaces, *Phys. Rev. Lett.* **98**, 146401 (2007).
- [19] M. Rupp, A. Tkatchenko, K.-R. Müller, and O. A. von Lilienfeld, Fast and Accurate Modeling of Molecular Atomization Energies with Machine Learning, *Phys. Rev. Lett.* **108**, 058301 (2012).
- [20] A. P. Bartók, R. Kondor, and G. Csányi, On representing chemical environments, *Phys. Rev. B* **87**, 184115 (2013).
- [21] J. Behler, Constructing high-dimensional neural network potentials: A tutorial review, *International Journal of Quantum Chemistry* **115**, 1032 (2015).
- [22] D. Marchand, A. Jain, A. Glensk, and W. A. Curtin, Machine learning for metallurgy I. A neural-network potential for Al-Cu, *Phys. Rev. Mater.* **4**, 103601 (2020).
- [23] C. Fan, M. Shen, Z. Nussinov, Z. Liu, Y. Sun, and Y.-Y. Liu, Searching for spin glass ground states through deep reinforcement learning, *Nature Communications* **14**, 725 (2023).
- [24] K. Mills and I. Tamblin, Deep neural networks for direct, featureless learning through observation: The case of two-dimensional spin models, *Phys. Rev. E* **97**, 032119 (2018).
- [25] J.-L. Wu, H. Xiao, and E. Paterson, Physics-informed machine learning approach for augmenting turbulence models: A comprehensive framework, *Phys. Rev. Fluids* **3**, 074602 (2018).
- [26] M. Raissi, P. Perdikaris, and G. Karniadakis, Physics-informed neural networks: A deep learning framework for solving forward and inverse problems involving nonlinear partial differential equations, *Journal of Computational Physics* **378**, 686 (2019).
- [27] S. L. Brunton, B. R. Noack, and P. Koumoutsakos, Machine Learning for Fluid Mechanics, *Annual Review of Fluid Mechanics* **52**, 477 (2020).
- [28] L. Lu, X. Meng, Z. Mao, and G. E. Karniadakis, DeepXDE: A Deep Learning Library for Solving Differential Equations, *SIAM Review* **63**, 208 (2021).
- [29] M. Mattheakis, P. Protopapas, D. Sondak, M. D. Giovanni, and E. Kaxiras, Physical Symmetries Embedded in Neural Networks (2020).
- [30] A. Bogatskiy, B. Anderson, J. Offermann, M. Roussi, D. Miller, and R. Kondor, Lorentz group equivariant neural network for particle physics, in *Proceedings of the 37th International Conference on Machine Learning*, Proceedings of Machine Learning Research, Vol. 119 (PMLR, 2020) pp. 992–1002.
- [31] L. Yang, D. Zhang, and G. E. Karniadakis, Physics-Informed Generative Adversarial Networks for Stochastic Differential Equations, *SIAM Journal on Scientific Computing* **42**, A292 (2020).
- [32] K. Mills, K. Ryczko, I. Luchak, A. Domurad, C. Beeler, and I. Tamblin, Extensive deep neural networks for transferring small scale learning to large scale systems, *Chem. Sci.* **10**, 4129 (2019).
- [33] S. Batzner, A. Musaelian, L. Sun, M. Geiger, J. P. Mailoa, M. Kornbluth, N. Molinari, T. E. Smidt, and B. Kozinsky, E(3)-equivariant graph neural networks for data-efficient and accurate interatomic potentials, *Nature Communications* **13**, 2453 (2022).
- [34] F. Xie, T. Lu, S. Meng, and M. Liu, GPTFF: A high-accuracy out-of-the-box universal AI force field for arbitrary inorganic materials, *Science Bulletin* **69**, 3525 (2024).
- [35] Y. Han, J. Wang, C. Ding, H. Gao, S. Pan, Q. Jia, and J. Sun, Prediction of surface reconstructions using MAGUS, *The Journal of Chemical Physics* **158**, 174109 (2023).
- [36] Y. Zhong, H. Yu, X. Gong, and H. Xiang, A General Tensor Prediction Framework Based on Graph Neural Networks, *The Journal of Physical Chemistry Letters* **14**, 6339 (2023).
- [37] H. Gao, J. Wang, Y. Han, and J. Sun, Enhancing crystal structure prediction by decomposition and evolution schemes based on graph theory, *Fundamental Research* **1**, 466 (2021).
- [38] J. Wang, H. Gao, Y. Han, C. Ding, S. Pan, Y. Wang, Q. Jia, H.-T. Wang, D. Xing, and J. Sun, MAGUS: machine learning and graph theory assisted universal structure searcher, *National Science Review* **10**, nwad128 (2023).
- [39] H. Yu, Y. Zhong, L. Hong, C. Xu, W. Ren, X. Gong, and H. Xiang, Spin-dependent graph neural network potential for magnetic materials, *Phys. Rev. B* **109**, 144426 (2024).
- [40] S.-H. Li and L. Wang, Neural Network Renormalization Group, *Phys. Rev. Lett.* **121**, 260601 (2018).
- [41] Y. Zhong, S. Liu, B. Zhang, Z. Tao, Y. Sun, W. Chu, X.-G. Gong, J.-H. Yang, and H. Xiang, Accelerating the calculation of electron-phonon coupling strength with

- machine learning, *Nature Computational Science* **4**, 615 (2024).
- [42] C. Zhang, Y. Zhong, Z.-G. Tao, X. Qing, H. Shang, Z. Lan, O. V. Prezhdo, X.-G. Gong, W. Chu, and H. Xiang, Advancing nonadiabatic molecular dynamics simulations for solids: Achieving supreme accuracy and efficiency with machine learning (2024).
- [43] H. Yu, C. Xu, X. Li, F. Lou, L. Bellaiche, Z. Hu, X. Gong, and H. Xiang, Complex spin Hamiltonian represented by an artificial neural network, *Phys. Rev. B* **105**, 174422 (2022).
- [44] T. Lv, Z. Zhong, Y. Liang, F. Li, J. Huang, and R. Zheng, Deep Charge: Deep learning model of electron density from a one-shot density functional theory calculation, *Phys. Rev. B* **108**, 235159 (2023).
- [45] Z. Fan, Y. Wang, P. Ying, K. Song, J. Wang, Y. Wang, Z. Zeng, K. Xu, E. Lindgren, J. M. Rahm, A. J. Gabourie, J. Liu, H. Dong, J. Wu, Y. Chen, Z. Zhong, J. Sun, P. Erhart, Y. Su, and T. Ala-Nissila, GPUMD: A package for constructing accurate machine-learned potentials and performing highly efficient atomistic simulations, *The Journal of Chemical Physics* **157**, 114801 (2022).
- [46] X.-T. Xie, Z.-X. Yang, D. Chen, Y.-F. Shi, P.-L. Kang, S. Ma, Y.-F. Li, C. Shang, and Z.-P. Liu, Lasp to the future of atomic simulation: Intelligence and automation, *Precision Chemistry* **2**, 612 (2024).
- [47] Z.-X. Yang, X.-T. Xie, P.-L. Kang, Z.-X. Wang, C. Shang, and Z.-P. Liu, Many-Body Function Corrected Neural Network with Atomic Attention (MBNN-att) for Molecular Property Prediction, *Journal of Chemical Theory and Computation* **20**, 6717 (2024).
- [48] L. Barroso-Luque, M. Shuaibi, X. Fu, B. M. Wood, M. Dzamba, M. Gao, A. Rizvi, C. L. Zitnick, and Z. W. Ulissi, Open materials 2024 (omat24) inorganic materials dataset and models (2024).
- [49] Y. Han, J. Wang, C. Ding, H. Gao, S. Pan, Q. Jia, and J. Sun, Prediction of surface reconstructions using MAGUS, *The Journal of Chemical Physics* **158**, 174109 (2023).
- [50] D. Pfau, J. S. Spencer, A. G. D. G. Matthews, and W. M. C. Foulkes, Ab initio solution of the many-electron Schrödinger equation with deep neural networks, *Phys. Rev. Res.* **2**, 033429 (2020).
- [51] C. Zener, Interaction between the d -Shells in the Transition Metals. II. Ferromagnetic Compounds of Manganese with Perovskite Structure, *Phys. Rev.* **82**, 403 (1951).
- [52] P. W. Anderson and H. Hasegawa, Considerations on Double Exchange, *Phys. Rev.* **100**, 675 (1955).
- [53] P. G. de Gennes, Effects of Double Exchange in Magnetic Crystals, *Phys. Rev.* **118**, 141 (1960).
- [54] J. Liu, H. Shen, Y. Qi, Z. Y. Meng, and L. Fu, Self-learning Monte Carlo method and cumulative update in fermion systems, *Phys. Rev. B* **95**, 241104 (2017).
- [55] M. A. Ruderman and C. Kittel, Indirect Exchange Coupling of Nuclear Magnetic Moments by Conduction Electrons, *Phys. Rev.* **96**, 99 (1954).
- [56] T. Kasuya, A Theory of Metallic Ferro- and Antiferromagnetism on Zener's Model, *Progress of Theoretical Physics* **16**, 45 (1956).
- [57] K. Yosida, Magnetic Properties of Cu-Mn Alloys, *Phys. Rev.* **106**, 893 (1957).
- [58] Supplemental Material of Effective field Neural Network.
- [59] *Renormalization Group and Effective Field Theory Approaches to Many-Body Systems*, 1st ed. (Springer Berlin, Heidelberg, 2012).
- [60] A. D. Becke, Density-functional exchange-energy approximation with correct asymptotic behavior, *Phys. Rev. A* **38**, 3098 (1988).
- [61] G. A. Baker and P. Graves-Morris, *Padé Approximants*, 2nd ed. (Cambridge University Press, Cambridge, 1996).
- [62] C. M. Bender and S. A. Orszag, *Advanced Mathematical Methods for Scientists and Engineers I*, 1st ed. (Springer New York, New York, NY, 1999).
- [63] G. Martin, The unreasonable effectualness of continued function expansions, *Journal of the Australian Mathematical Society* **77**, 305–320 (2004).
- [64] V. Abhignan and R. Sankaranarayanan, Continued Functions and Perturbation Series: Simple Tools for Convergence of Diverging Series in $O(n)$ -Symmetric ϕ^4 Field Theory at Weak Coupling Limit, *Journal of Statistical Physics* **183**, 4 (2021).
- [65] C. M. Bender and J. P. Vinson, Summation of power series by continued exponentials, *Journal of Mathematical Physics* **37**, 4103 (1996).
- [66] D. Poland, Summation of series in statistical mechanics by continued exponentials, *Physica A: Statistical Mechanics and its Applications* **250**, 394 (1998).
- [67] K. He, X. Zhang, S. Ren, and J. Sun, Deep Residual Learning for Image Recognition, in *2016 IEEE Conference on Computer Vision and Pattern Recognition (CVPR)* (IEEE Computer Society, 2016) pp. 770–778.
- [68] S. Xie, R. Girshick, P. Dollár, Z. Tu, and K. He, Aggregated Residual Transformations for Deep Neural Networks, in *2017 IEEE Conference on Computer Vision and Pattern Recognition (CVPR)* (IEEE Computer Society, 2017) pp. 5987–5995.
- [69] S. Zagoruyko and N. Komodakis, Wide Residual Networks (2017).
- [70] G. Huang, Z. Liu, L. Van Der Maaten, and K. Q. Weinberger, Densely Connected Convolutional Networks, in *2017 IEEE Conference on Computer Vision and Pattern Recognition (CVPR)* (IEEE Computer Society, 2017) pp. 2261–2269.